Enhanced anticorrosion performance of zinc rich epoxy coatings modified with stainless steel flakes

Qi, Chunping; Dam-Johansen, Kim; Weinell, Claus Erik; Bi, Huichao; Wu, Hao

Published in:
Progress in Organic Coatings

Link to article, DOI:
10.1016/j.porgcoat.2021.106616

Publication date:
2022

Document Version
Publisher's PDF, also known as Version of record

Progress in Organic Coatings 163 (2022) 106616

Contents lists available at ScienceDirect

Progress in Organic Coatings

journal homepage: www.elsevier.com/locate/porgcoat

Enhanced anticorrosion performance of zinc rich epoxy coatings modified with stainless steel flakes

Chunping Qi [a], Kim Dam-Johansen [a,b], Claus Erik Weinell [a], Huichao Bi [a], Hao Wu [b,*]

[a] The Hempel Foundation Coatings Science and Technology Centre (CoaST), Department of Chemical and Biochemical Engineering, Technical University of Denmark, Building 229, 2800 Kgs. Lyngby, Denmark
[b] CHEC Research Center, Department of Chemical and Biochemical Engineering, Technical University of Denmark, Building 229, 2800 Kgs. Lyngby, Denmark

ARTICLE INFO

Keywords:
Corrosion
EIS
Stainless steel flakes
Zinc-rich coating

ABSTRACT

The effect of a partial replacement of spherical zinc particles by stainless steel flakes (SSF) on the corrosion protection performance of zinc-rich epoxy (ZRE) coating was studied. Salt spray test, open circuit potential, electrochemical impedance spectroscopy and potentiodynamic polarization tests were utilized to evaluate the anticorrosion performance of the coatings. The results demonstrate that a partial replacement of zinc particles by SSF enhanced the anticorrosion properties of the ZRE coating, and the enhancement was attributed to the synergistic effects by increasing the coating impedance and extending the cathodic protection duration.

1. Introduction

Zinc-rich coatings, which contain metallic zinc particles (usually spherical zinc dust) and a binder system (such as epoxy and inorganic silicates), have been successfully applied since 1930s for the corrosion protection of steel surfaces, and they are still one of the most effective and widely used anticorrosive coatings in industrial and marine environments [1,2].

The main corrosion protection mechanism of a zinc-rich coating during the early stage of its service life is cathodic protection. The effect of cathodic protection is decayed with time due to the formation of nonconductive corrosion products, but meanwhile an enhanced barrier protection is provided by the corrosion products sealing the micropores and cracks inside the coating [3]. The cathodic protection of a zinc-rich coating depends mainly on the zinc content and the morphology of zinc particles [4]. Typically, a zinc content of $\geq$80 wt% is required for a good electrical contact of zinc-to-zinc particles inside the coating and the zinc-to-steel substrate at the interface, which is essential for a high cathodic protection performance [5–7]. Nevertheless, such a high loading of zinc particles could result in a decreased mechanical integrity of the coating (low cohesive strength), poor mechanical properties such as crack propagation and weak adhesion to the steel substrate, difficulties in spraying due to high viscosity and poor dispersion, and segmentation of zinc during storage [8]. Besides, less use of zinc and zinc compounds is favored environmentally due to their toxicity to aquatic life. Considering these facts together with the relatively low utilization rate of zinc during its service time, in recent years, several strategies have been used to improve anticorrosion performance and/or reduce the zinc content of zinc-rich coatings such as promoting the electrical conductivity by electroconducting additives [9,10], enhancing the barrier properties by hydrophobic/inhibitive additives or lamellar shape materials [11–13], and decreasing the oxidation rate of zinc particles by surface modification [14]. The surface modification reduces the electrochemical activity of zinc particles by forming a complex layer on their surface, while the presence of lamellar pigments reduces zinc corrosion rate by hindering the electrolyte penetration; therefore, both strategies can prolong the cathodic protection duration of zinc-rich coatings [13,15].

It has been reported that replacing a small part of zinc microparticles with Zn or Al nanoparticles promoted the electrical contact by filling the free space between the zinc microparticles and therefore enhanced cathodic protection properties of a zinc-rich coating [16,17]. In addition, nonmetallic nanoparticles such as clay nanolayers, SiO_2, and TiO_2 nanoparticles, have been utilized to improve the anticorrosion performance of zinc-rich coatings by enhancing the barrier property and other physico-mechanical properties such as hardness and adhesion to the substrate [18–20].

To improve the electrical conductivity and thus the utilization rate of zinc particles in the zinc-rich coatings, addition of electrically conductive materials has been put forward. The intrinsically conducting

* Corresponding author.
E-mail address: haw@kt.dtu.dk (H. Wu).

https://doi.org/10.1016/j.porgcoat.2021.106616
Received 20 September 2021; Received in revised form 12 November 2021; Accepted 12 November 2021
Available online 19 November 2021

polymers, such as polyaniline (PAni), polypyrrole and their derivatives, have been reported to enhance the electrical conductivity of the coatings and inhibit surplus sacrificial galvanic and self-corrosion of the zinc particles [8,21,22]. Armelin et al. [23] found that by incorporating 0.3 wt% of conductive PAni emeraldine salt, the zinc content in the zinc-rich epoxy (ZRE) coating could be reduced from 79 wt% to 60 wt% without detrimental effects on its corrosion protection properties. Additionally, many carbon based additives such as carbon black [24], graphite [8], carbon fibers [25], biochar [26], carbon nanotubes (CNTs) [6,27,28] and graphene [2,29–31] have been reported to improve the anticorrosion performance of zinc-rich coatings. Particularly, a synergetic enhancement of barrier protection and cathodic protection was usually achieved in the case of zinc-rich coating containing CNTs or graphene nanosheets because of their excellent electrical conductivity and barrier property [9,10,32]. In recent years, reduced graphene oxide has been developed to solve the problem of inhomogeneous dispersion caused by strong Van der Waals forces and large surface areas of graphene nanosheets [33,34]. Nevertheless, a counter-effect on the coating performance has been reported due to the formation of microgalvanic cells between the carbon-based material and steel substrate. Therefore, an efficient distribution of the electrical current needs to be ensured to prevent localized attack in the steel surface [6,35].

Further, several studies have employed conductive fillers such as diiron phosphide (Fe_2P) to improve the electrical conductivity, or lamellar fillers such as micaceous iron oxide (MIO) and lamellar Al particles to improve the barrier property, via a partial replacement of spherical zinc particles in zinc-rich coatings [13,36]. Arman et al. [13] reported that a replacement of 10 wt% zinc particles by 10 wt% MIO enhanced the anticorrosion properties of ZRE coating without reducing its sacrificial properties. However, the influence of Fe_2P on the anticorrosive properties of zinc-rich coatings are highly dependent on the binder used. Feliu et al. [37] reported that it was possible to replace up to 25 wt% of zinc particles with Fe_2P in ethyl silicate zinc-rich coatings without compromising their coatings properties. However, in the case of ZRE coating, a partial replacement of zinc particles with Fe_2P always resulted in a substantial reduction in the cathodic protection period, since Fe_2P could accelerate the activation and corrosion rate of zinc particles. The effect was counteracted with the introduction of silane by reducing the activation and corrosion rate of zinc particles. Therefore, a synergy effect with respect to enhanced cathodic protection and barrier protection was obtained with the addition of 6 wt% Fe_2P and 0.4 wt% silane to the ZRE coating [38].

In summary, the incorporation of non-conductive particles though improves the barrier or inhibitive effect but usually reduces the electrical conductivity of the coating film and thus the cathodic protection. The presence of conductive fillers improves the cathodic protection, but may accelerate the oxidation of zinc due to the galvanic coupling between zinc particles and the conductive fillers. Finding a material to improve both cathodic protection and barrier property simultaneously and without destroying each other is still a major challenge in the ZRE coating especially at reduced zinc content. Stainless steel flakes (SSF), being widely used in decorative coatings to offer a metallic appearance and having a high hardness and strong rust-proofing effect, can be a potential conductive filler in anticorrosive coatings. To the best of our knowledge, no work has been performed on the incorporation of SSF into the zinc-rich coatings. In this work, SSF were investigated as a conductive filler to partially replace zinc particles in the ZRE coating. The anticorrosion performance of the coatings was evaluated using accelerated salt spray test. Evolution of the anticorrosion performance was also characterized by spectroscopy techniques, surface morphology techniques, and electrochemical techniques to improve the mechanistic understandings.

Table 1
Main components of the coatings investigated in this study.

Sample	Zinc (wt%)	SSF (wt%)	Binder (wt%)	PVC (%)
85ZRE	85	0	15	47.6
2.5SSF-80ZRE	80	2.5	17.5	43.3
5SSF-75ZRE	75	5	20	39.9
10SSF-66ZRE	66	10	24	34.2

2. Experimental

2.1. Preparation and application of coatings

Zinc particles, with an average diameter of 13 μm, were provided by EverZinc Norway AS. SSF with a nominal diameter of 26 μm were purchased from ECKART GmbH. The particle morphology and size distribution of zinc particles and SSF are displayed in Fig. S1 in Supplementary Materials. The ZRE coating, which contains 85 wt% of zinc particles, was prepared by mixing the zinc particles together with epoxy resin (with polyamide as a curing agent), solvent and other ingredients such as dispersants, rheological agents and deformer using an ultrasonic mixer. The ZRE coatings containing SSF were prepared by substituting a part of zinc particles with SSF, while keeping the pigment volume concentration (PVC)/critical pigment volume concentration (CPVC) ratio constant (PVC/CPVC = 0.74). The as-prepared coatings are denoted as 85ZRE, 2.5SSF-80ZRE, 5SSF-75ZRE and 10SSF-66ZRE, respectively, by the weight percentages of SSF and zinc particles. The main components and their contents in different coatings are listed in Table 1.

The as-prepared coatings were applied with a 150 μm gap applicator on a cleaned sandblasted (Sa 2½) S235JR steel surfaces (150 mm × 75 mm). The coated samples were left curing for 7 days under room temperature and humidity prior to testing. The thickness of the dry films measured by using an Elcometer gauge was 95 ± 10 μm for all samples.

2.2. Salt spray test

To evaluate the anticorrosion performance, salt spray test was performed on the coated samples. The edges and backsides of panels were protected by a commercial epoxy coating and the coated surface was scratched with a scribe-making machine to 2 mm wide and 50 mm long to expose the bare steel. Following ISO 9227 [39], the scribed, coated samples were placed into a salt spray chamber and exposed to a continuous spraying of 5% NaCl solution at 35 °C for a period of 2160 h (90 days). The experiments were carried out in triplicate for each formulation.

After 2160 h salt spray test, all samples were evaluated with respect to rust creepage at scribe. Around the scribe, the loose coating induced by underfilm corrosion was removed with a blade. The width of visible corrosion was measured at nine points according to Fig. 1. The maximum and average rust creep were calculated by [40]:

$$\text{Maximum rust creep}: c_{max} = \frac{w_{max} - w_0}{2} \quad (1)$$

$$\text{Average rust creep}: c_{av} = \frac{w_{av} - w_0}{2} \quad (2)$$

where w_{max} and w_{av} is the maximum and average of the nine widths measured, respectively, and w_0 is the original width (i.e., 2 mm) of the artificial scribe.

2.3. Characterization

X-ray diffraction (XRD) and attenuated total reflection-fourier transform infrared spectroscopy (ATR-FTIR) were used to analyze the corrosion products formed after salt spray test. The morphologies, pigments distribution of samples before and after salt spray test were

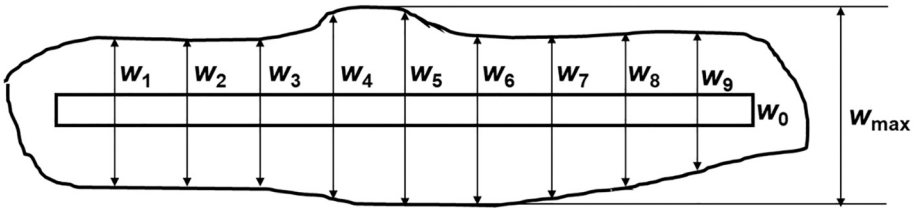

Fig. 1. Determination of average and maximum scribe creep. The artificial scribe has an original width of 2 mm and length of 50 mm. The width of visible corrosion was measured at nine points, including the midpoint of the scribe line and four points with 5 mm apart on each side of the midpoint.

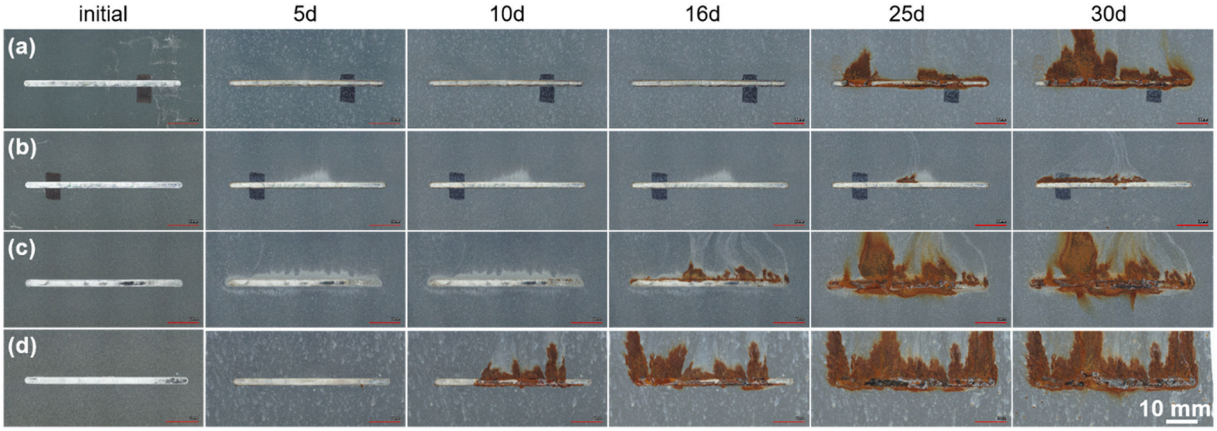

Fig. 2. Photographs of unmodified and SSF-modified ZRE coatings after exposure in salt spray chamber: (a) 85ZRE; (b) 2.5SSF-80ZRE; (c) 5SSF-75ZRE; (d) 10SSF-66ZRE.

examined using a scanning electron microscope (SEM) at an accelerating voltage of 20 keV. Elemental content in the different samples was determined by energy dispersive spectroscopy (EDS).

2.4. Electrochemical performance tests

The electrochemical behavior of coatings was analyzed by electrochemical impedance spectroscopy (EIS) and the Tafel polarization test using a Gamry Potentiostat Reference 600+. A three-electrode system was used, employing the coated panel as working electrode with an exposed area of 10 cm^2, a graphite rod as counter electrode and a saturated calomel electrode (SCE) as a reference electrode. The EIS measurement was performed at room temperature (25 °C) in 3.5 wt %-NaCl solution over a frequency range of 10 mHz to 100 kHz, with an acquisition rate of 10 points per decade, with a signal amplitude of 10 mV at the open circuit potential (OCP). The measurements were conducted on the two replicates to ensure the repeatability of data. The obtained EIS data was analyzed using the software ZsimpWin. Potentiodynamic polarization test was performed at early stage of immersion to investigate the corrosion of zinc by scanning the electrode potential from −150 to +150 mV at a scanning rate of 0.167 mV/s.

3. Results and discussions

3.1. Salt spray test

The visual performance of unmodified and SSF-modified ZRE coatings after salt spray exposure is shown in Fig. 2. Owning to the galvanic activity, the accumulation of white (zinc) corrosion products formed near the scribes was more pronounced on the 2.5SSF-80ZRE and 5SSF-75ZRE coatings. This indicates a small loading of SSF facilitated the activation of zinc particles near the scribed areas. After long time exposure, red rust was formed at scribed area which indicates that the active zinc particles near scribe were consumed and could no longer

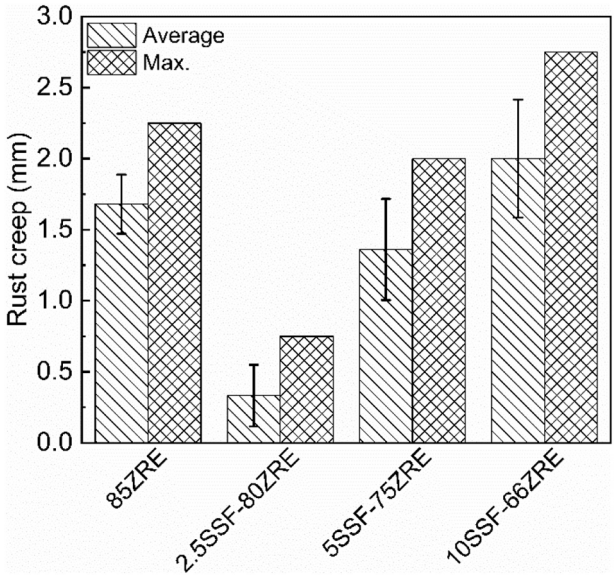

Fig. 3. Scribe creep measured for different coatings after 90 days salt spray test.

provide cathodic protection for the exposed steel. However, the corrosion of underlying steel was inhibited by the formed zinc corrosion products. The best corrosion protection performance was obtained for the 2.5SSF-80ZRE coating. With the increasing amount of SSF, the sample exhibited shorter cathodic protection duration accompanied by the formation of more red rust. A few small blisters were visually observed on the intact surface areas of the unmodified 85ZRE coating, while no blister was observed on the surface of the coatings containing SSF. Many white spots, formed from the self-corrosion of zinc particles

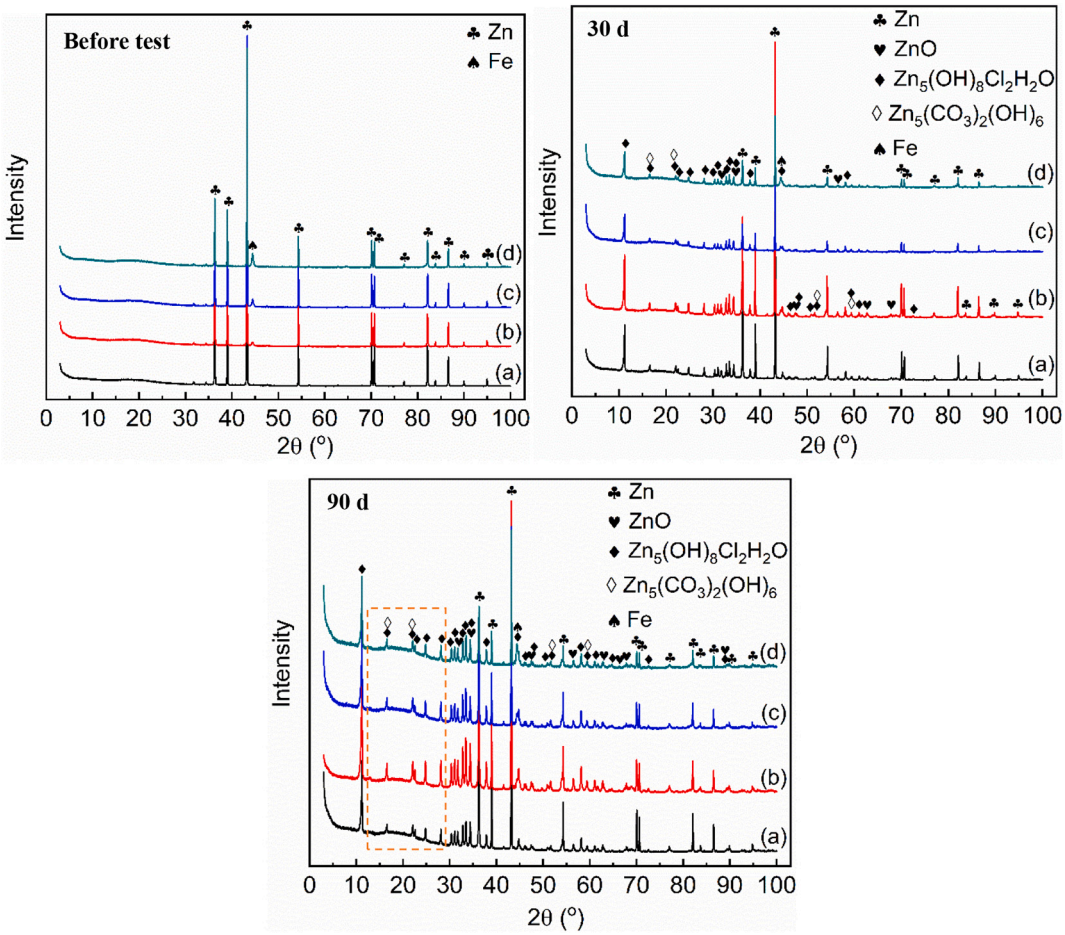

Fig. 4. XRD patterns of different coatings before and after salt spray test: (a) 85ZRE; (b) 2.5SSF-80ZRE; (c) 5SSF-75ZRE; (d) 10SSF-66ZRE.

due to the direct contact with the corrosive media, were observed on the surface (intact areas) of 85ZRE and 10SSF-66ZRE coatings. This may be because 85ZRE has a high porosity due to the high total pigment contents (with spherical particles only), while 10SSF-66ZRE has a poor packing/wetting due to the high loading of big flakes, and also the galvanic coupling between zinc particles and SSF may accelerate the zinc oxidation. The replicate results of salt spray test are shown in Fig. S2 in Supplementary Materials, which show a good replicability and demonstrate that replacing zinc particles with a small amount (2.5–5.0 wt%) of SSF enhanced the anticorrosion performance of the ZRE coating.

After 90 days salt spray test, the rust creep resistance was evaluated and the result is shown in Fig. 3. A minimum value of 0.33 mm is seen for the average rust creep of the 2.5SSF-80ZRE coating, besides, both 2.5SSF-80ZRE and 5SSF-75ZRE coatings have less rust creep than the 85ZRE coating, indicating a better long-term corrosion protection performance. However, with the increase of SSF content, the coating in general showed more rust creep (both average and maximum scribe creep).When the content of SSF increased to 10 wt%, the coating exhibited most rust creep among all coatings, indicating a poor anticorrosion performance.

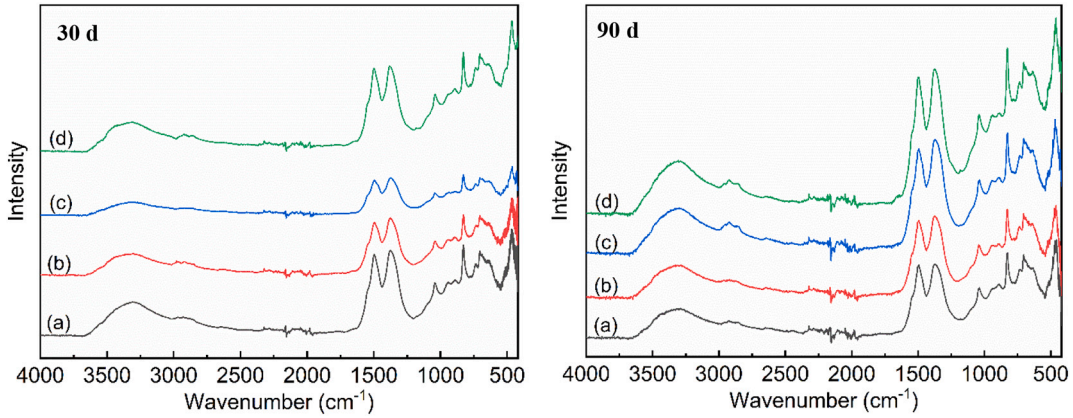

Fig. 5. ATR-FTIR spectra of coated samples surface after salt spray test: (a) 85ZRE; (b) 2.5SSF-80ZRE; (c) 5SSF-75ZRE; (d) 10SSF-66ZRE.

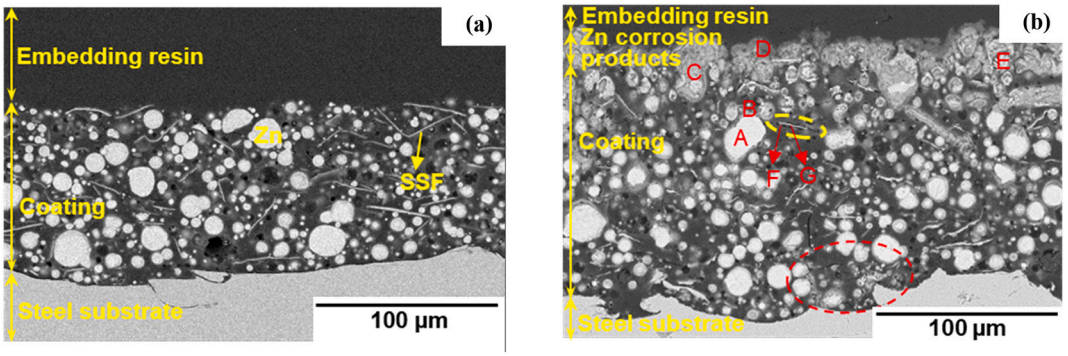

Fig. 6. Cross-section SEM images of the 2.5SSF-80ZRE coating (a) before and (b) after 30 days salt spray test: A: unattacked zinc, B-G: corrosion products, and F: unattacked SSF were regions where EDS analysis was performed. (The observed black vacancies were caused by the zinc particles leaving the surface when polishing.)

3.2. XRD and FTIR characterization of corrosion products

To further investigate the corrosion process on steel, the composition of corrosion products was characterized using XRD and ATR-FTIR.

XRD patterns of the powdered samples scrapped from steel panels are exhibited in Fig. 4. Before exposure, all coatings displayed only diffraction peaks associated with metallic zinc in addition to a small peak attributed to iron when SSF was incorporated. After exposure, in addition to the dominant peaks corresponding to metallic Zn, the XRD spectra of all coatings showed prevailing contributions from simonkolleite $Zn_5(OH)_8Cl_2{\cdot}H_2O$ with small contributions from hydrozincite $Zn_5(CO_3)_2(OH)_6$ and zincite ZnO. This is in good agreement with the composition of zinc corrosion products reported in the literature [38,41]. With the exposure time extending to 90 days, the relative intensity of peaks associated with the corrosion products increased significantly, which indicates an incremental accumulation of zinc corrosion products. The other three samples exhibited a more pronounced small hump centered at $2\theta = 20^{\circ}$ which is attributed to the amorphous zinc corrosion products, whereas the 2.5SSF-80ZRE coating showed relatively higher intensity of sharp peaks, indicating a formation of a higher amount of crystalline corrosion products.

The ATR-FTIR spectra were applied to study the corrosion products formed on the outer coating surface after salt spray test. As shown in Fig. 5, the spectra of all coatings show the same main peaks and vibration bands, indicating the formation of identical corrosion products on the outer surface of all coatings. The bands at 1506 cm^{-1}, 1387 cm^{-1}, 1050 cm^{-1}, 833 cm^{-1} and 707 cm^{-1} suggest the presence of carbonate groups. The separation of the bands 1506 and 1387 cm^{-1} indicates a high degree of crystallinity. Further, the broad band at 3324 cm^{-1} is attributed to the O—H stretching vibration, and the broadening is because of the formation of hydrogen-bond between CO_3^{2-} and H_2O molecules in the interlayer. The aforementioned bands indicate the formation of $Zn_5(CO_3)_2(OH)_6$ [42]. Additionally, the characteristic absorption band at 465 cm^{-1} is attributed to the Zn—O stretching vibration in ZnO [43]. Stronger intensity peaks were observed for the 85ZRE and 10SSF-66ZRE coatings after 30 days salt spray test, indicating an increased formation of $Zn_5(CO_3)_2(OH)_6$ on the coating outer surface due to the higher porosity, which is consistent with the visual appearance of more "white" corrosion products (Fig. 2 (a) and (d)). With longer exposure time, all coatings exhibited increased intensity of bands due to the increased formation of $Zn_5(CO_3)_2(OH)_6$ and ZnO.

Different from XRD patterns, chloride containing corrosion products (e.g. $Zn_5(OH)_8Cl_2{\cdot}H_2O$) were not detected in the ATR-FTIR spectra. This is because the soluble chloride ions (Cl^-) are usually washed off on the outer surface, and the chloride-containing corrosion products are therefore mostly accumulated at the zinc/corrosion product layer interface inside the coating film [44], however, the penetration depth into the sample by using ATR is typically between 0.5 and 2 μm [45]. This was further confirmed by the EDS results.

Table 2
EDS results at indicated locations in SEM cross-section images of the 2.5SSF-80ZRE coating after 30 days salt spray test (unit: wt%[a]).

Region	C	O	Cl	Cr	Mn	Fe	Zn	Mo
A	4.2	0.9				0.6	94.4	
B	11.7	6.5	13.9			0.7	66.3	
C	6.5	15.4	15.4			0.3	61.8	0.6
D	19.4	13.0	1.5			0.4	63.7	0.7
E	4.9	12.9	1.1			0.5	80.2	0.5
F	14.8	0.9	1.7	11.6	7.3	53.9	5.8	2.9
G	16.3	1.8	12.6	0.4	0.1	1.5	65.3	0.6

[a] Elements with a content below 1.0 wt% is not shown in the table.

3.3. SEM-EDS analysis

SEM-EDS was applied to further understand the mechanism of corrosion protection. Fig. 6 depicts the cross-section SEM images of the 2.5SSF-80ZRE coating before and after salt spray test. The cross-section SEM images of the other three coated samples (i.e., 85ZRE, 5SSF-75ZRE, and 10SSF-66ZRE coatings) and their corresponding EDS elemental mapping images after test are displayed in Fig. S3 in Supplementary Materials. Before exposure, it is seen that the spherical zinc particles and the sheet-like SSF were uniformly distributed. With the increase of SSF content, more SSF with less zinc particles were observed across the coating layer, and no obvious sedimentation of big/heavy particles were observed. SSF tend to align randomly but mostly in parallel with the steel surface, making diffusion paths of corrosive media more tortuous to reach the steel substrate. After 30 days salt spray test, a barrier layer of zinc corrosion products was formed on the outer surface of all coatings, which is also indicated by the EDS oxygen mapping images (Fig. S3) with oxygen-rich coating surfaces. In addition, a thinner layer of zinc corrosion product was observed with the increase of SSF content, which suggests the coating has a decreased cathodic protection capability. EDS analysis was performed in regions A, B, C, D, E, F, and G, and the results are reported in Table 2. The EDS results of the other three coatings are reported in Table S1 in Supplementary Materials. The images and EDS results show that most of the zinc particles (see bright spots like spot A) inside the coating were unattacked, whereas in some defective areas (see areas like spot B), the ingress of salt water and corrosion of zinc were found as evidenced by the EDS result of a high Cl content and the rings of oxygen and chloride surrounding zinc particles (Fig. S3). A slightly severer attack of the zinc particles that are in contact with the steel substrate (see particles within the red circles) were observed locally due to their sacrificial corrosion to protect steel substrate. Further, the presence of SSF provides cathodic sites for oxygen reduction, and according to the EDS results in regions F and G, a few zinc corrosion

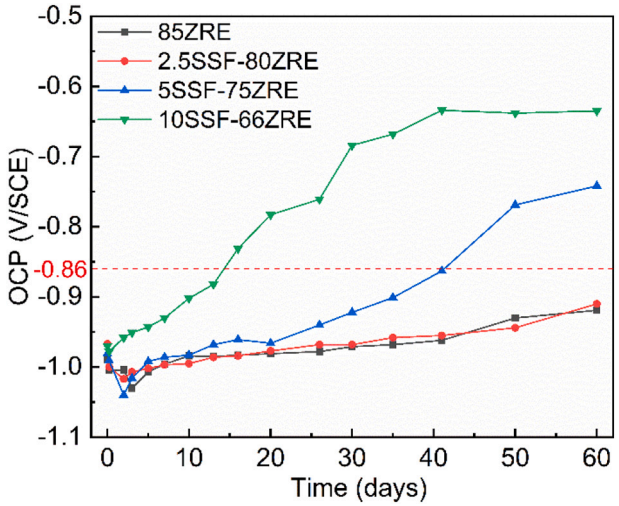

Fig. 7. OCP evolution of different coatings during 60 days immersion in 3.5 wt % NaCl solution. The dotted line (−0.86 V) represents the thermodynamic protection limit, below which coating provides cathodic protection.

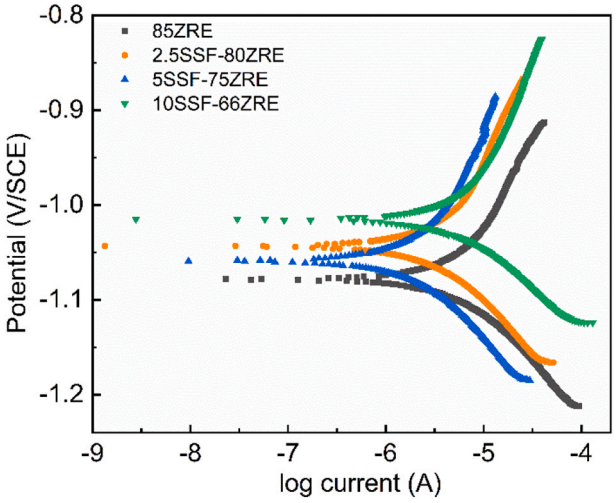

Fig. 8. Tafel polarization plots for steel coated with the four coatings after 1 day immersion in 3.5 wt% NaCl solution.

products were precipitated on the surface of SSF, whereas SSF themselves were not corroded. As indicated in Fig. S3 and Table S1, the other three samples show similar corrosion behavior to the 2.5SSF-80ZRE coating, i.e., only zinc particles were sacrificially corroded to protect the steel substrate, and similar distribution of different zinc corrosion products were formed across the coating layer. Further, the formation of rust layer at the coating/steel interface was not detected, implying that all coatings provided corrosion protection to the steel substrate after 30 days salt spray test. Additionally, the corrosion products inside the coating were mostly simonkolleite, whereas different Zn/O/Cl ratios are found in regions C, D, and E suggesting that the barrier layer is a combination of different zinc corrosion products, which is also confirmed by the XRD and ATR-FTIR results.

3.4. Electrochemical characterization of the coated samples

3.4.1. Open circuit potential measurements

OCP measurement is widely used to characterize the cathodic protection ability and duration of zinc-rich coatings. Based on the previous studies [46,47], it has been commonly accepted that the criterion for cathodic protection of iron in acid and neutral solutions is an OCP less than −0.86 V/SCE, a value corresponding to the criterion of a maximum Fe^{2+} concentration of 10^{-6} mol/L, and the potential should be less negative than −1.143 V/SCE to avoid the occurrence of hydrogen evolution [47,48]. The corrosion potential of zinc and uncoated steel in a NaCl solution is approximately −1.05 V/SCE and − 0.65 V/SCE, respectively [49]. The measured OCP is a mixed potential in between those of the immersed zinc particles and steel substrate, and the potential magnitude depends on the relative active zinc-to-steel area ratio. An increase in potential corresponds to a decrease of the zinc-to-steel area ratio, indicating a decrease of the cathodic protection intensity [47].

The OCP evolutions of different coated samples in neutral 3.5 wt% NaCl solution at 25 °C are shown in Fig. 7. As observed in Fig. 7, all samples, except the 10SSF-66ZRE coating, exhibited a decreasing potential magnitude period in the first 5 days immersion. This is related to the activation of the zinc particles and an increase in the zinc-to-steel area ratio. Subsequently, a gradual positive shift of OCP values occurred due to the corrosion of zinc particles and the isolation of zinc particles by the nonconductive corrosion products. The OCP evolution of the 10SSF-66ZRE coating shifted to the positive direction significantly faster as compared to the other three coatings, indicating a faster penetration of water due to the high porosity, causing the zinc particles wetted and corroded very fast. The OCP values (<−0.86 V/SCE) of both 2.5SSF-80ZRE and 85ZRE coatings remained in cathodic protection region during the entire 60 days immersion test. However, a further increasing replacement of the zinc particles by SSF was accompanied by a large reduction in the cathodic protection duration. This is because, on the one hand, SSF has inherently more positive potential, and on the other hand, the galvanic coupling between zinc and SSF may accelerate the activation and corrosion of zinc particles in the coating. With a further increase of SSF content, the OCP becomes positive, and thereby shortening the cathodic protection duration. The replicate measurements show consistent result (Fig. S4 in Supplementary Materials). Further, the result agrees well with the salt spray test result, and it is consistent with result reported in the literature when zinc particles were partially replaced by Fe_2P [37].

Table 3
Potentiodynamic polarization parameters derived by Tafel region extrapolation from the polarization plots shown in Fig. 8.

Sample	E_{corr} (V/SCE)	I_{corr} (μA·cm^{-2})	β (V/dec)	R_p (kΩ·cm^2)
85ZRE	−1.080	0.594	0.217	36.4
2.5SSF-80ZRE	−1.040	0.437	0.237	54.2
5SSF-75ZRE	−1.060	0.222	0.204	91.8
10SSF-66ZRE	−1.020	0.620	0.228	36.7

3.4.2. Tafel polarization measurements

To investigate the corrosion behavior of zinc within the coating at early stage of immersion, potentiodynamic polarization test was performed after one day immersion when all the coated samples exhibited a potential below the cathodic protection limit (−0.86 V/SCE). Fig. 8 shows the Tafel polarization plots of steel panel coated with the four different coatings. The corresponding corrosion potential (E_{corr}), corrosion current density (I_{corr}), and polarization resistance (R_p) values are listed in Table 3. The polarization resistance is related to the corrosion current density and calculated according to the Stern-Geary equation [50]:

$$R_p = \frac{\beta}{I_{corr}} \quad (3)$$

where β is the Stern Geary constant.

All samples exhibited a more negative potential value than −0.86 V/SCE, which indicates that zinc particles behave actively to provide cathodic protection to the steel substrate at the beginning. Further, the

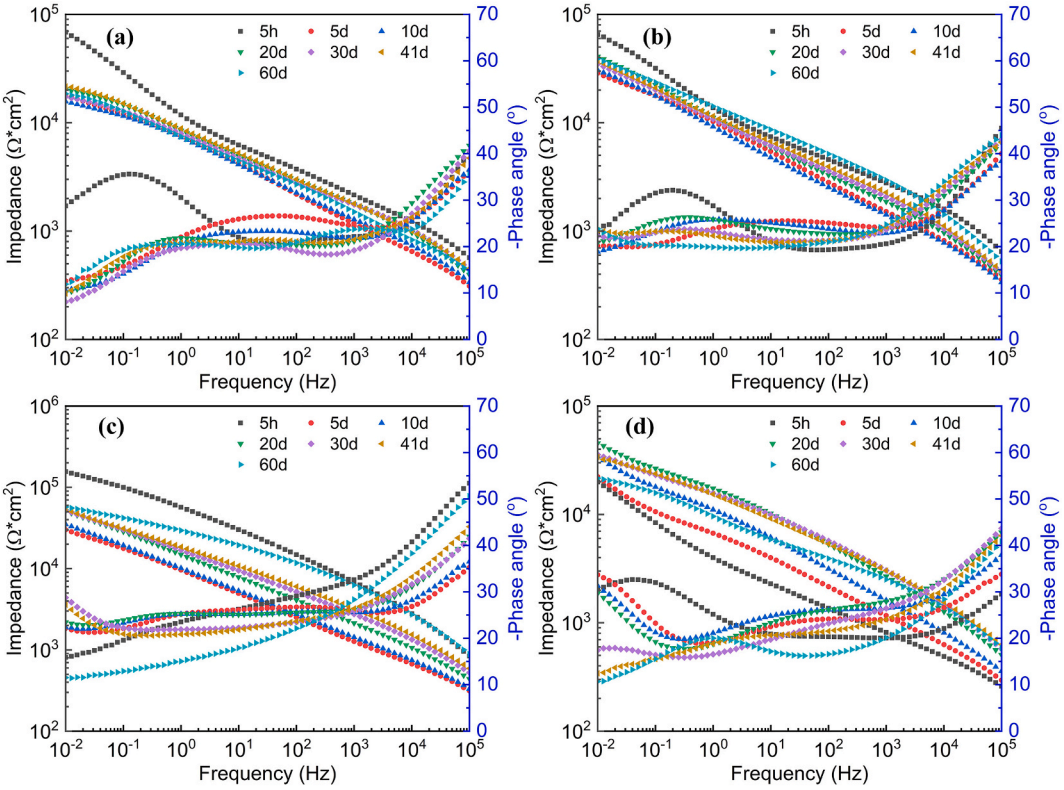

Fig. 9. Bode plots of different coatings during 60 days immersion in 3.5 wt% NaCl solution: (a) 85ZRE; (b) 2.5SSF-80ZRE; (c) 5SSF-75ZRE; (d) 10SSF-66ZRE.

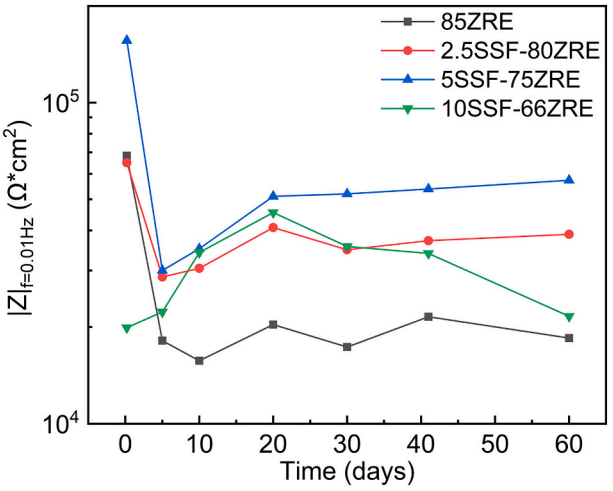

Fig. 10. Impedance value of different coatings at lowest measured frequency ($|Z|_{f=0.01\ Hz}$) during 60 days immersion in 3.5 wt% NaCl solution.

low corrosion current value accompanied by the high polarization resistance value presented by the 2.5SSF-80ZRE and 5SSF-75ZRE coatings indicated a low dissolution rate of zinc particles at the initial cathodic protection stage. This is in good agreement with the high charge transfer resistance and coating resistance obtained from the EIS measurements, which will be discussed later in Section 3.4.3.

3.4.3. EIS measurements

EIS measurement was used to study the corrosion reaction and barrier property of coatings. For organic coatings, the impedance modulus at lowest frequency ($|Z|_{f=0.01\ Hz}$) is commonly used to qualitatively evaluate the barrier property to the steel substrate. It is generally recognized that the higher the $|Z|_{0.01Hz}$ value, the better is the protection performance of the coating, and the more quickly the $|Z|_{0.01Hz}$ value drops, the faster the coating degrades [51]. The impedance-Bode plots and evolution of $|Z|_{f=0.01\ Hz}$ value of different coated samples are exhibited in Figs. 9 and 10, respectively. As seen in Fig. 10, the initial $|Z|_{f=0.01\ Hz}$ value ranked in an order: 5SSF-75ZRE > 2.5SSF-80ZRE ≈ 85ZRE > 10SSF-66ZRE, indicating a denser coating film was obtained with zinc particles replaced by a small amount of SSF. In terms of the 85ZRE coating, the Bode-impedance value decreased dramatically from 68390 Ω·cm^2 to 18140 Ω·cm^2 after 5 days immersion, and then leveled off at around 20000 Ω·cm^2 during the remaining test periods, implying an insufficient filling of coating porosities by the corrosion products and thus a poor corrosion resistance. In contrast, both the 2.5SSF-80ZRE and 5SSF-75ZRE coatings exhibited a dramatic decrease (to approximately 30000 Ω·cm^2) in the values of impedance in the first 5 days immersion due to water uptake, but then the impedance values increased gradually to 39000 Ω·cm^2 and 57000 Ω·cm^2, respectively due to the formation of zinc corrosion products. This result show that during 60 days immersion test, the 5SSF-75ZRE coating exhibited the best barrier property, followed by the 2.5SSF-80ZRE coating, both of which were better than the unmodified 85ZRE coating, demonstrating that an appropriate amount of SSF can enhance the corrosion resistance of the ZRE coating. The impedance of the 10SSF-66ZRE coating increased in the first 20 days immersion due to the formation of zinc corrosion products; however, the impedance decreased after 20 days, indicating an initiated corrosion of underlying steel substrate. The result is consistent with the increased OCP due to the corrosion of zinc at very early time of exposure. Moreover, some blisters were observed on the coating surface after 41 days immersion, suggesting that the coating had lost its corrosion protection ability.

The Nyquist impedance diagrams for different coatings obtained in 3.5% NaCl solution as a function of immersion time are shown in Fig. 11. From the perspective of coating structure, the electrolyte could reach the surface of zinc particles rapidly to react. This effect resulted in the

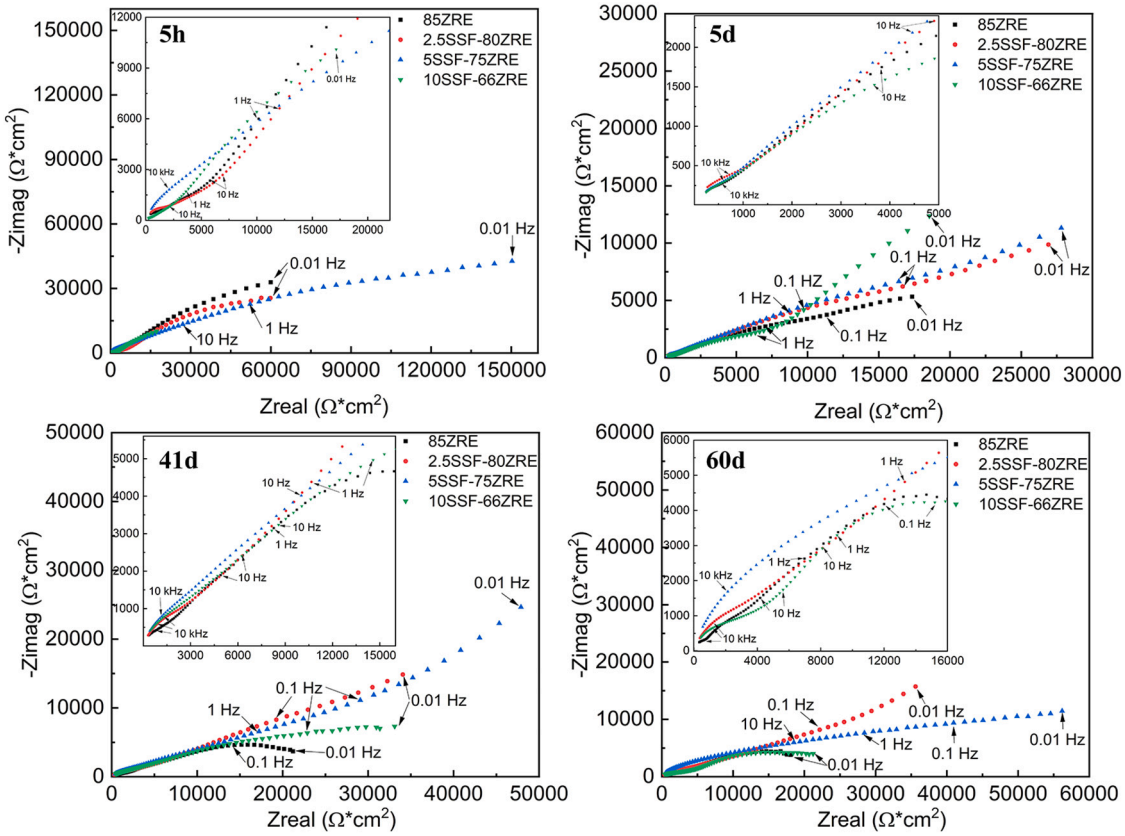

Fig. 11. Nyquist plots of different coatings during 60 days immersion in 3.5 wt% NaCl solution.

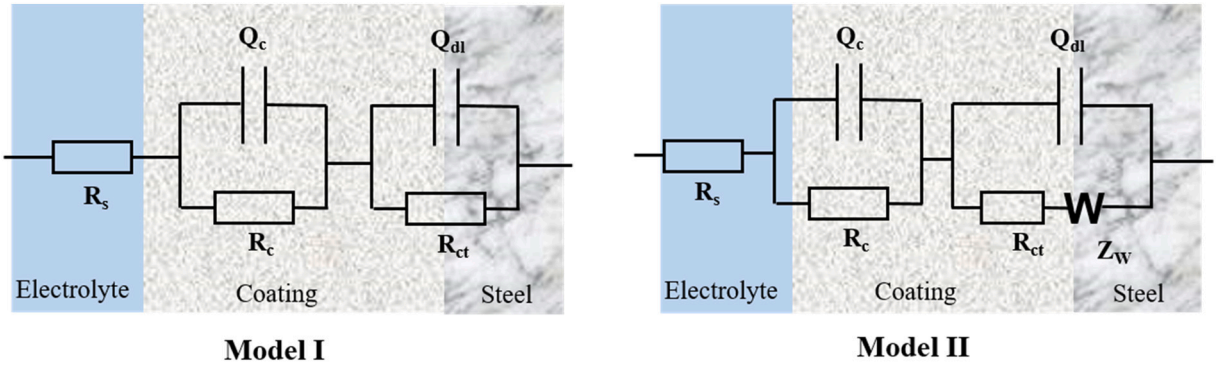

Fig. 12. Equivalent circuits used to model electrochemical behavior of coated specimens.

emergence of two time constants (two depressed arcs) at the beginning of immersion test in Fig. 11. The high-frequency loop represents the impedance and capacitance of the coating, and the low-frequency one corresponds to the zinc dissolution reaction at early stage and the corrosion process taking place at the coating/steel interface at late stage. The diameter of low-frequency arcs in the Nyquist plots for all samples decreased rapidly from 5 h to 5 d, which reflects the rapid penetration of electrolyte into ZRE coatings with high zinc content. The decrease of the diameter of the semicircles in the earlier stage of immersion is in agreement with the rapid decrease of corrosion potentials as shown in Fig. 7. Further, for the 85ZRE coating, two distinct arcs were observed over the entire test period, and the low-frequency loop was more pronounced than the high-frequency one, indicating an enhancement in activation and dissolution of zinc particles. In addition to the two depressed arcs, a diffusion tail was observed in the Nyquist plots of the 2.5SSF-ZRE and 5SSF-75ZRE coatings in the late stage of immersion, because the formed zinc corrosion products could fill the micropores in the coating and reduce the porosities. In contrast, a pronounced diffusion tail was observed until 41 days immersion for the 10SSF-66ZRE coating, accompanied by the formation of some small blisters, indicating the loss of protection ability.

As shown in Figs. 9 and 11, the results revealed that all coatings demonstrated a Bode plot with two time constants and Nyquist plot with two capacitive arcs, which could be considered as a clear evidence that electrolyte has penetrated through the coating film and the corrosion reaction has initiated. Therefore, the Randles equivalent circuit model, with additional double layer capacitor and charge transfer resistor connected parallel as shown in Fig. 12, was used to fit the EIS results and interpret the corrosion process of the coating. In the equivalent circuit models, R_s is the electrolyte resistance, R_c is the coating film resistance, and Q_c is the constant phase element (CPE) of the coating. R_{ct} and Q_{dl} represent the charge transfer resistance and electrical double-layer

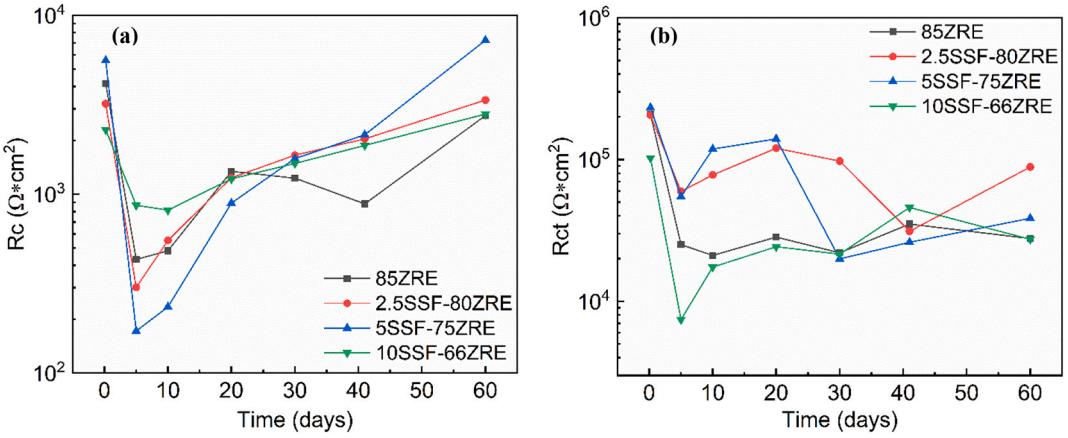

Fig. 13. Evolution of (a) coating resistance and (b) charge transfer resistance over immersion time of different coatings.

constant phase element of zinc dissolution (at early stage of exposure) at the zinc-electrolyte interface and corrosion at the steel/coating interface (at late stage of exposure). Warburg element Z_w is taken to represent diffusion impedance for the diffusion-controlled corrosion reaction process. Considering the surface heterogeneity and pigments dispersion effects, CPE is introduced to describe the surface roughness and the frequency dependence of nonideal capacitive behavior [41]. Model I without W was used to fit the EIS spectra in the early stage of immersion for all samples except the 10SSF-ZRE coating that exhibited a diffusion tail after 5 h immersion due to the presence of high content of SSF. At late stage of immersion, Model II with W was used to fit the EIS spectra of the 2.5SSF-80ZRE and 5SSF-75ZRE coatings because of the enhanced barrier effect by the formation of corrosion products. However, the 10SSF-66ZRE coating lost its protective ability after 41 days immersion, and the EIS spectra was fitted using Model I.

After equivalent electric circuit fitting, the evolution of coating resistance and charge transfer resistance over immersion time is shown in Fig. 13. As seen in Fig. 13 (a), the R_c variation of all coatings had similar trend with immersion time. The R_c value of coatings declined quickly until the change was stopped at 5 days, which agrees well with the OCP evolution, indicating the water had completely penetrate into the coating film and zinc particles were activated. Subsequently, with the formed corrosion products sealing the coating micropores, the R_c value increased gradually during the remaining immersion time. Since the magnitude of R_c is bound up with the amount of the porosity of the coating and the diffusion situation of the corrosive species in the coating, the result indicates the 2.5SSF-80ZRE and 5SSF-75ZRE coatings provided better barrier protection than the 85ZRE coating at late stage of the exposure time. Furthermore, it is seen from Fig. 13 (b), early on, R_{ct} values of all coatings decreased as a result of the dissolution of the zinc particles. The R_{ct} values then increased along with the formation of zinc corrosion products. Moreover, the R_{ct} values of the 2.5SSF-80ZRE and 5SSF-75ZRE coatings remained at a higher level than that of the 85ZRE coating during the entire immersion test, which means a significantly high corrosion resistance. At early stage of immersion, the evolution of higher R_{ct} values, which are largely derived from better protectiveness for zinc particles from well-dispersed SSF, indicating a lower electrochemical activity of zinc particles and thus a slower consumption rate. At the late stage of immersion, the R_{ct} value serves as the corrosion activity at the coating/steel interface, and the evolution of higher R_{ct} values implies a higher resistance to the steel corrosion. Additionally, consistent results were obtained when comparing R_c and R_{ct} variations by fitting the results of replicate EIS measurements (Fig. S5 in Supplementary Materials), which indicates that the 2.5SSF-80ZRE and 5SSF-75ZRE coatings provided enhanced barrier protection and improved corrosion resistance compared to the 85ZRE coating.

In summary, the electrochemical test results indicated that S235JR steel coated with 2.5SSF-80ZRE and 5SSF-75ZRE coatings possessed a better impedance value and cathodic protection ability, which manifested as the superior corrosion protection performance. The results are consistent with the salt spray test result: compared with the 85ZRE coating, 2.5SSF-80ZRE and 5SSF-75ZRE coatings exhibited overall enhanced corrosion protection properties in terms of red rust formation and rust creep at scribes.

3.5. Discussion of corrosion protection mechanisms

The corrosion of zinc and the formation of corrosion products are highly dependent on the temperature and corrosive environment such as the corrosive species and pH. The XRD, FTIR and SEM-EDS results indicated that the main corrosion products of all coatings were $Zn_5(OH)_8Cl_2{\cdot}H_2O$, $Zn_5(CO_3)_2(OH)_6$ and ZnO. With the exposure time increased, corrosion products precipitated continuously on the surfaces.

Based on literature [44,52], the zinc corrosion starts with the anodic zinc dissolution (Eq. (4)) and cathodic oxygen reduction (Eq. (5)). The released Zn^{2+} ions then migrate to cathodic sites and buffer them by the formation of $Zn(OH)_2$ (Eq. (6)). Zincate ions can be produced owning to the localized slightly alkaline pH at cathodic sites (Eq. (8)), and it undergoes additional conversion to ZnO (Eq. (9)). The slightly soluble zinc oxides/hydroxides could further react with CO_2 absorbed or dissolved from the environment into the electrolyte and Cl^- ions to form insoluble complex corrosion products such as hydrozincite (Eqs. (10)–(12)) and simonkolleite (Eq. (13)) at various parts depending on pH, Cl^- ion concentration and the concentration of dissolved CO_2.

$$Zn \rightarrow Zn^{2+} + 2e^- \quad (4)$$

$$O_2 + 4e^- + 2H_2O \rightarrow 4OH^- \quad (5)$$

$$Zn^{2+} + 2\,OH^- \rightarrow Zn(OH)_2 \quad (6)$$

$$Zn(OH)_2 \rightarrow ZnO + H_2O \quad (7)$$

$$Zn(OH)_2 + 2OH^- \rightarrow Zn(OH)_4^{2-} \quad (8)$$

$$Zn(OH)_4^{2-} \rightarrow ZnO + 2OH^- + H_2O \quad (9)$$

$$5Zn(OH)_2 + 2CO_2 \rightarrow Zn_5(CO_3)_2(OH)_6 + 2H_2O \quad (10)$$

$$5ZnO + 3H_2O + 2CO_2 \rightarrow Zn_5(CO_3)_2(OH)_6 \quad (11)$$

$$5Zn(OH)_4^{2-} + 2CO_2 \rightarrow Zn_5(CO_3)_2(OH)_6 + 10OH^- + 2H_2O \quad (12)$$

$$5Zn(OH)_2 + 2Cl^- + H_2O \rightarrow Zn_5(OH)_8Cl_2{\cdot}H_2O + 2OH^- \quad (13)$$

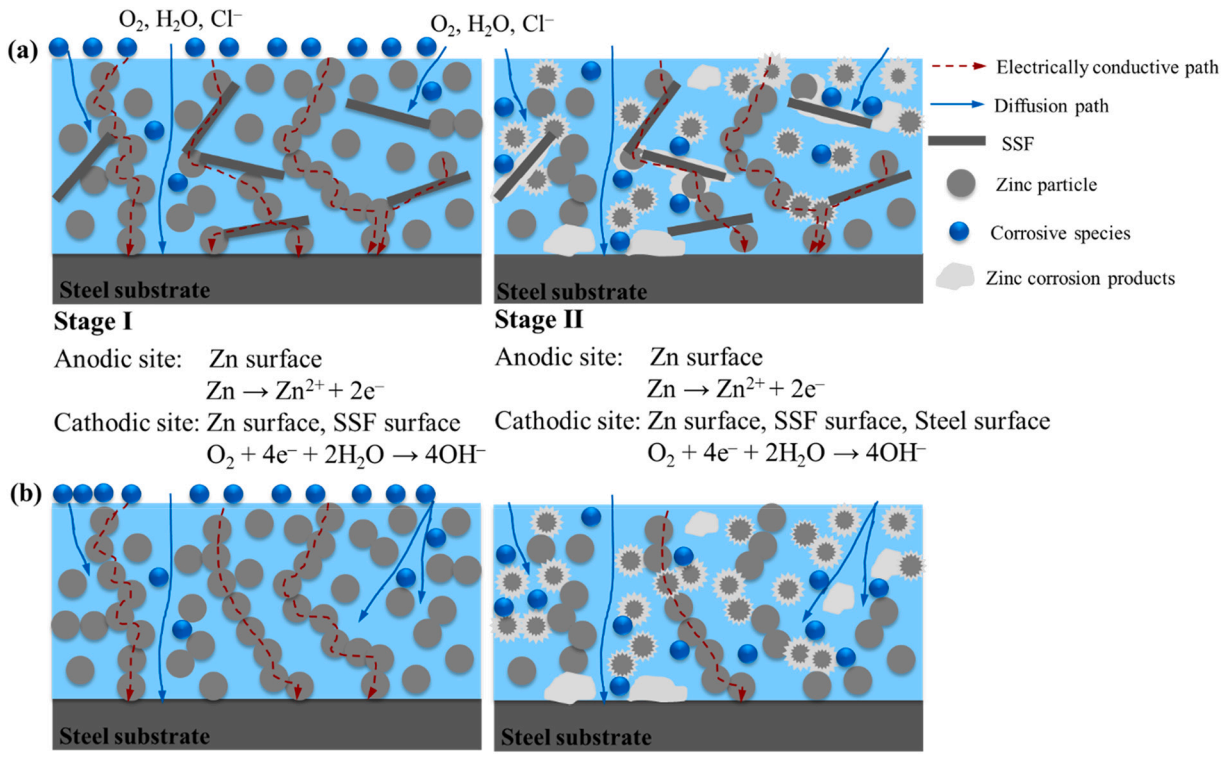

Fig. 14. Schematic diagram of corrosion protection mechanism of the ZRE coating (a) with and (b) without SSF.

For the ZRE coating without SSF, initially, both the anodic zinc dissolution (Eq. (4)) and cathodic oxygen reduction (Eq. (5)) take place on the surface of zinc particles. With the increasing exposure time, the dissolved oxygen diffuses to the steel substrate and cathodic oxygen reduction takes place on the steel surface as well. The formation of nonconductive zinc corrosion products isolates the zinc particles from each other and from the steel substrate, and the cathodic protection is decayed due to the loss of electrical connectivity. The incorporation of SSF into the ZRE coating provides many cathodic sites for the oxygen reduction, and a few zinc corrosion products are accumulated on the surface of SSF (see EDS results in regions F and G within yellow circles in Fig. 6), with less anodic sites (surface of zinc particles) covered by the corrosion products. As a result, there is a less anodic polarization of the zinc particles and therefore, the cathodic protection period is more extensive. In addition, SSF acts as a 'bridge' and increases the utilization rate of zinc by connecting more isolated zinc particles into conductive percolation paths. On the other hand, the presence of lamellar SSF could improve the physical barrier effect by making diffusion paths of corrosive species more tortuous to reach the steel substrate and meanwhile the oxidation rate of zinc particles is reduced. The schematic diagram of corrosion protection mechanism of the ZRE coating with and without SSF is shown in Fig. 14.

4. Conclusions

Part of zinc particles in the ZRE coating was replaced by SSF at different levels. The coatings loaded with 2.5 and 5.0 wt% SSF exhibited a good anticorrosion performance with no blisters on the surface and less rust creep at scribes. The OCP evolution confirmed that the coating containing 2.5 wt% SSF remained under cathodic protection for a long time. According to the EIS measurements, the presence of 2.5 wt% and 5 wt% of SSF could provide an enhanced barrier protection against corrosive media and thereby providing a less aggressive environment for corrosion of zinc particles and steel substrate. The same corrosion products, i.e., $Zn_5(OH)_8Cl_2{\cdot}H_2O$, $Zn_5(CO_3)_2(OH)_6$, and ZnO were characterized in the unmodified and SSF-modified coatings, whereas more crystallized corrosion products were formed in the coating with 2.5 wt% SSF, which results in better corrosion protection during the late stage.

CRediT authorship contribution statement

Chunping Qi: Conceptualization, Methodology, Validation, Formal analysis, Investigation, Data curation, Writing – original draft. **Kim Dam-Johansen:** Conceptualization, Methodology, Writing – review & editing, Supervision, Project administration, Funding acquisition. **Claus Erik Weinell:** Conceptualization, Methodology, Writing – review & editing, Supervision, Project administration. **Huichao Bi:** Validation, Writing – review & editing. **Hao Wu:** Conceptualization, Methodology, Writing – review & editing, Supervision, Project administration.

Declaration of competing interest

The authors declare that they have no known competing financial interests or personal relationships that could have appeared to influence the work reported in this paper.

Acknowledgements

This work is financially supported by Hempel Foundation and China Scholarship Council. The authors would like to thank Alicia Gutierrez Garcia for her assistance with the formulation design and technical discussions.

Appendix A. Supplementary data

Supplementary data to this article can be found online at https://doi.org/10.1016/j.porgcoat.2021.106616.

References

[1] X.G. Zhang, Chapter 12. Zinc-Rich Coatings, in: Corros. Electrochem. Zinc, Springer Science & Business Media, 1996, pp. 337–349.

[2] X. Cao, F. Huang, C. Huang, J. Liu, Y.F. Cheng, Preparation of graphene nanoplate added zinc-rich epoxy coatings for enhanced sacrificial anode-based corrosion protection, Corros. Sci. 159 (2019) 108120, https://doi.org/10.1016/j.corsci.2019.108120.

[3] F. Theiler, The rust preventing mechanism of zinc dust paints, Corros. Sci. 14 (1974), https://doi.org/10.1016/0010-938X(74)90001-8.

[4] J.R. Vilche, E.C. Bucharsky, C.A. Giúdice, Application of EIS and SEM to evaluate the influence of pigment shape and content in ZRP formulations on the corrosion prevention of naval steel, Corros. Sci. 44 (2002) 1287–1309, https://doi.org/10.1016/S0010-938X(01)00144-5.

[5] S. Shreepathi, P. Bajaj, B.P. Mallik, Electrochemical impedance spectroscopy investigations of epoxy zinc rich coatings: role of Zn content on corrosion protection mechanism, Electrochim. Acta 55 (2010) 5129–5134, https://doi.org/10.1016/j.electacta.2010.04.018.

[6] Y. Cubides, H. Castaneda, Corrosion protection mechanisms of carbon nanotube and zinc-rich epoxy primers on carbon steel in simulated concrete pore solutions in the presence of chloride ions, Corros. Sci. 109 (2016) 145–161, https://doi.org/10.1016/j.corsci.2016.03.023.

[7] N. Hammouda, H. Chadli, G. Guillemot, K. Belmokre, The corrosion protection behaviour of zinc rich epoxy paint in 3% NaCl solution, Adv. Chem. Eng. Sci. 1 (2011) 51–60, https://doi.org/10.4236/aces.2011.12009.

[8] A. Kalendová, D. Veselý, M. Kohl, J. Stejskal, Anticorrosion efficiency of zinc-filled epoxy coatings containing conducting polymers and pigments, Prog. Org. Coatings. 78 (2015) 1–20, https://doi.org/10.1016/j.porgcoat.2014.10.009.

[9] Y. Lei, Z. Qiu, J. Liu, D. Li, N. Tan, T. Liu, Y. Zhang, X. Chang, Y. Gu, Y. Yin, Effect of conducting polyaniline/graphene nanosheet content on the corrosion behavior of zinc-rich epoxy primers in 3.5% NaCl solution, Polymers (Basel) 11 (2019), https://doi.org/10.3390/polym11050850.

[10] E. Langer, M. Zubielewicz, H. Kuczyńska, A. Królikowska, L. Komorowski, Anticorrosive effectiveness of coatings with reduced content of Zn pigments in comparison with zinc-rich primers, Corros. Eng. Sci. Technol. 54 (2019) 627–635, https://doi.org/10.1080/1478422X.2019.1652428.

[11] K. Kowalczyk, T. Spychaj, Zinc-free varnishes and zinc-rich paints modified with ionic liquids, Corros. Sci. 78 (2014) 111–120, https://doi.org/10.1016/j.corsci.2013.09.006.

[12] H. Hayatdavoudi, M. Rahsepar, Smart inhibition action of layered double hydroxide nanocontainers in zinc-rich epoxy coating for active corrosion protection of carbon steel substrate, J. Alloys Compd. 711 (2017) 560–567, https://doi.org/10.1016/j.jallcom.2017.04.044.

[13] S.Y. Arman, B. Ramezanzadeh, S. Farghadani, M. Mehdipour, A. Rajabi, Application of the electrochemical noise to investigate the corrosion resistance of an epoxy zinc-rich coating loaded with lamellar aluminum and micaceous iron oxide particles, Corros. Sci. 77 (2013) 118–127, https://doi.org/10.1016/j.corsci.2013.07.034.

[14] J.H. Park, T.H. Yun, K.Y. Kim, Y.K. Song, J.M. Park, The improvement of anticorrosion properties of zinc-rich organic coating by incorporating surface-modified zinc particle, Prog. Org. Coatings. 74 (2012) 25–35, https://doi.org/10.1016/j.porgcoat.2011.09.012.

[15] T.H. Yun, J.H. Park, J.S. Kim, J.M. Park, Effect of the surface modification of zinc powders with organosilanes on the corrosion resistance of a zinc pigmented organic coating, Prog. Org. Coatings. 77 (2014) 1780–1788, https://doi.org/10.1016/j.porgcoat.2014.06.008.

[16] K. Schaefer, A. Miszczyk, Improvement of electrochemical action of zinc-rich paints by addition of nanoparticulate zinc, Corros. Sci. 66 (2013) 380–391, https://doi.org/10.1016/j.corsci.2012.10.004.

[17] M. Jalili, M. Rostami, B. Ramezanzadeh, An investigation of the electrochemical action of the epoxy zinc-rich coatings containing surface modified aluminum nanoparticle, Appl. Surf. Sci. 328 (2015) 95–108, https://doi.org/10.1016/j.apsusc.2014.12.034.

[18] F.T. Shirehjini, I. Danaee, H. Eskandari, D. Zarei, Effect of nano clay on corrosion protection of zinc-rich epoxy coatings on steel 37, J. Mater. Sci. Technol. 32 (2016) 1152–1160, https://doi.org/10.1016/j.jmst.2016.08.017.

[19] A. Anandhi, S. Palraj, G. Subramanian, M. Selvaraj, Corrosion resistance and improved adhesion properties of propargyl alcohol impregnated mesoporous titanium dioxide built-in epoxy zinc rich primer, Prog. Org. Coatings. 97 (2016) 10–18, https://doi.org/10.1016/j.porgcoat.2016.03.003.

[20] M. Zhang, H. Wang, T. Nie, J. Bai, F. Zhao, Enhancement of barrier and anti-corrosive performance of zinc-rich epoxy coatings using nano-silica/graphene oxide hybrid, Corros. Rev. 38 (2020) 497–513, https://doi.org/10.1515/corrrev-2020-0034.

[21] A. Gergely, É. Pfeifer, I. Bertóti, T. Török, E. Kálmán, Corrosion protection of cold-rolled steel by zinc-rich epoxy paint coatings loaded with nano-size alumina supported polypyrrole, Corros. Sci. 53 (2011) 3486–3499, https://doi.org/10.1016/j.corsci.2011.06.014.

[22] E. Akbarinezhad, Synthesis of conductive polyaniline-graphite nanocomposite in supercritical CO2 and its application in zinc-rich epoxy primer, J. Supercrit. Fluids 94 (2014) 8–16, https://doi.org/10.1016/j.supflu.2014.06.018.

[23] E. Armelin, M. Martí, F. Liesa, J.I. Iribarren, C. Alemán, Partial replacement of metallic zinc dust in heavy duty protective coatings by conducting polymer, Prog. Org. Coatings. 69 (2010) 26–30, https://doi.org/10.1016/j.porgcoat.2010.04.023.

[24] H. Marchebois, S. Touzain, S. Joiret, J. Bernard, C. Savall, Zinc-rich powder coatings corrosion in sea water: influence of conductive pigments, Prog. Org. Coatings. 45 (2002) 415–421, https://doi.org/10.1016/S0300-9440(02)00145-5.

[25] T. Ge, W. Zhao, X. Wu, X. Lan, Y. Zhang, Y. Qiang, Y. He, Incorporation of electroconductive carbon fibers to achieve enhanced anti-corrosion performance of zinc rich coatings, J. Colloid Interface Sci. 567 (2020) 113–125, https://doi.org/10.1016/j.jcis.2020.02.002.

[26] Z. Li, G. Ravenni, H. Bi, C. Erik, B. Ulusoy, Y. Zhang, K. Dam-johansen, Effects of biochar nanoparticles on anticorrosive performance of zinc-rich epoxy coatings, Prog. Org. Coat. 158 (2021) 106351, https://doi.org/10.1016/j.porgcoat.2021.106351.

[27] H. Castaneda, M. Galicia, Corrosion assessment of Zn-rich epoxy primers with carbon nanotube additions in an electrolyte with a bacteria consortium, Front. Mater. 6 (2019) 1–12, https://doi.org/10.3389/fmats.2019.00307.

[28] S. Cho, T.M. Chiu, H. Castaneda, Electrical and electrochemical behavior of a zinc-rich epoxy coating system with carbon nanotubes as a diode-like material, Electrochim. Acta 316 (2019) 189–201, https://doi.org/10.1016/j.electacta.2019.05.116.

[29] R. Ding, S. Chen, N. Zhou, Y. Zheng, B. Jun Li, T. Jiang Gui, X. Wang, W. Hua Li, H. Bin Yu, H. Wen Tian, The diffusion-dynamical and electrochemical effect mechanism of oriented magnetic graphene on zinc-rich coatings and the electrodynamics and quantum mechanics mechanism of electron conduction in graphene zinc-rich coatings, J. Alloys Compd. 784 (2019) 756–768, https://doi.org/10.1016/j.jallcom.2019.01.070.

[30] J. Liu, T. Liu, Z. Guo, N. Guo, Y. Lei, X. Chang, Y. Yin, Promoting barrier performance and cathodic protection of zinc-rich epoxy primer via single-layer graphene, Polymers (Basel) 10 (2018), https://doi.org/10.3390/polym10060591.

[31] S. Mohammadi, H. Roohi, Influence of functionalized multi-layer graphene on adhesion improvement and corrosion resistance performance of zinc-rich epoxy primer, Corros. Eng. Sci. Technol. 53 (2018) 422–430, https://doi.org/10.1080/1478422X.2018.1495679.

[32] M. Ehsanjoo, S. Mohammadi, N. Chaibakhsh, Long-term corrosion resistance of zinc-rich paint using functionalised multi-layer graphene-tripolyphosphate: in situ creation of zinc phosphate as corrosion inhibitor, Corros. Eng. Sci. Technol. 54 (2019) 698–714, https://doi.org/10.1080/1478422X.2019.1661132.

[33] S. Teng, Y. Gao, F. Cao, D. Kong, X. Zheng, X. Ma, L. Zhi, Zinc-reduced graphene oxide for enhanced corrosion protection of zinc-rich epoxy coatings, Prog. Org. Coat. 123 (2018) 185–189, https://doi.org/10.1016/j.porgcoat.2018.07.012.

[34] S. Zhou, Y. Wu, W. Zhao, J. Yu, F. Jiang, Y. Wu, L. Ma, Designing reduced graphene oxide/zinc rich epoxy composite coatings for improving the anticorrosion performance of carbon steel substrate, Mater. Des. 169 (2019) 107694, https://doi.org/10.1016/j.matdes.2019.107694.

[35] D. Wang, E. Sikora, B. Shaw, A comparison of the corrosion response of zinc-rich coatings with and without presence of carbon nanotubes under erosion and corrosion conditions, Corrosion 74 (2018) 1203–1213, https://doi.org/10.5006/2743.

[36] B. Ramezanzadeh, S.Y. Arman, M. Mehdipour, Anticorrosion properties of an epoxy zinc-rich composite coating reinforced with zinc, aluminum, and iron oxide pigments, J. Coat. Technol. Res. 11 (2014) 727–737, https://doi.org/10.1007/s11998-014-9580-0.

[37] S. Feliu, M. Morcillo, J.M. Bastidas, S. Feliu, Zinc reactivity in zinc-rich coatings co-pigmented with di-iron phosphide, J. Coatings Technol. 63 (1991) 31–34.

[38] D.M. Xie, K. Huang, X. Feng, Y.G. Wang, Improving the performance of zinc-rich coatings using conductive pigments and silane, Corros. Eng. Sci. Technol. 55 (2020) 539–549, https://doi.org/10.1080/1478422X.2020.1759484.

[39] B. STANDARD, B. ISO, Corrosion tests in artificial atmospheres—salt spray tests, 2006.

[40] H. Bi, C.E. Weinell, R. Agudo de Pablo, B. Santos Varela, S. González Carro, Á. Rodríguez Ruiz, K. Dam-Johansen, Rust creep assessment—A comparison between a destructive method according to ISO 12944 and selected non-destructive methods, Prog. Org. Coatings 157 (2021), https://doi.org/10.1016/j.porgcoat.2021.106293.

[41] X. Li, Y. Cubides, Z. He, M.D. Soucek, H. Castaneda, Corrosion assessment of zinc-rich primers containing polyaniline and the effect of acid as a dopant, Corrosion 74 (2018) 1141–1157, https://doi.org/10.5006/2769.

[42] F. Zhu, D. Persson, D. Thierry, C. Taxen, Formation of corrosion products on open and confined zinc surfaces exposed to periodic wet/dry conditions, Corrosion 56 (2000) 1256–1265.

[43] J. Winiarski, W. Tylus, K. Winiarska, I. Szczygieł, B. Szczygieł, XPS and FT-IR characterization of selected synthetic corrosion products of zinc expected in neutral environment containing chloride ions, J. Spectrosc. 2018 (2018), https://doi.org/10.1155/2018/2079278 Research.

[44] D. De la Fuente, J.G. Castaño, M. Morcillo, Long-term atmospheric corrosion of zinc, Corros. Sci. 49 (2007) 1420–1436, https://doi.org/10.1016/j.corsci.2006.08.003.

[45] M. Nagasawa, N. Okada, N. Otsuka, T. Ohtsuka, Corrosion process of inorganic zinc-rich painted steel exposed to a high-chloride atmospheric environment, ISIJ Int. 58 (2018) 316–322, https://doi.org/10.2355/isijinternational.ISIJINT-2017-548.

[46] Y. Cubides, S.S. Su, H. Castaneda, Influence of zinc content and chloride concentration on the corrosion protection performance of zinc-rich epoxy coatings containing carbon nanotubes on carbon steel in simulated concrete pore environments, Corrosion 72 (2016) 1397–1423, https://doi.org/10.5006/2104.

[47] C.M. Abreu, M. Izquierdo, M. Keddam, X.R. Novoa, H. Takenouti, Electrochemical behaviour of zinc-rich epoxy paints in 3% NaCl solution, Electrochim. Acta 41 (1996) 2405–2415, https://doi.org/10.1016/0013-4686(96)00021-7.

[48] C.M. Abreu, M. Izquierdo, P. Merino, X.R. Nóvoa, C. Pérez, A new approach to the determination of the cathodic protection period in zinc-rich paints, Corrosion 55 (1999) 1173–1181, https://doi.org/10.5006/1.3283955.
[49] O.Ø. Knudsen, U. Steinsmo, M. Bjordal, Zinc-rich primers - test performance and electrochemical properties, Prog. Org. Coatings. 54 (2005) 224–229, https://doi.org/10.1016/j.porgcoat.2005.06.009.
[50] M. Stern, A.L. Geary, Electrochemical polarization: I. A theoretical analysis of the shape of polarization curves, J. Electrochem. Soc. 104 (1957) 56.
[51] C. Xing, W. Wang, S. Qu, Y. Tang, X. Zhao, Y. Zuo, Degradation of zinc-rich epoxy coating in 3 . 5% NaCl solution and evolution of its EIS parameters, J. Coatings Technol. Res. 18 (2021) 843–860, https://doi.org/10.1007/s11998-020-00448-8.
[52] M. Mouanga, P. Berçot, J.Y. Rauch, Comparison of corrosion behaviour of zinc in NaCl and in NaOH solutions. Part I: Corrosion layer characterization, Corros. Sci. 52 (2010) 3984–3992, https://doi.org/10.1016/j.corsci.2010.08.003.